minerals

MDPI

Review

The Thermodynamics of Selenium Minerals in Near-Surface Environments

Vladimir G. Krivovichev [1,*], Marina V. Charykova [2] and Andrey V. Vishnevsky [2]

[1] Department of Mineralogy, Institute of Earth Sciences, St. Petersburg State University, 7/9 University Embankment, Saint Petersburg 199034, Russia

[2] Department of Geochemistry, Institute of Earth Sciences, St. Petersburg State University, 7/9 University Embankment, Saint Petersburg 199034, Russia; m-char@yandex.ru (M.V.C.); adrenalin1506@gmail.com (A.V.V.)

* Correspondence: vkrivovi@yandex.ru; Tel.: +7-812-328-9481

Received: 18 August 2017; Accepted: 4 October 2017; Published: 6 October 2017

Abstract: Selenium compounds are relatively rare as minerals; there are presently only 118 known mineral species. This work is intended to codify and systematize the data of mineral systems and the thermodynamics of selenium minerals, which are unstable (selenides) or formed in near-surface environments (selenites), where the behavior of selenium is controlled by variations of the redox potential and the acidity of solutions at low temperatures and pressures. These parameters determine the migration of selenium and its precipitation as various solid phases. All selenium minerals are divided into four groups—native selenium, oxide, selenides, and oxysalts—anhydrous selenites (I) and hydrous selenites and selenates (II). Within each of the groups, minerals are codified according to the minimum number of independent elements necessary to define the composition of the mineral system. Eh–pH diagrams were calculated and plotted using the Geochemist's Workbench (GMB 9.0) software package. The Eh–pH diagrams of the Me–Se–H_2O systems (where Me = Co, Ni, Fe, Cu, Pb, Zn, Cd, Hg, Ag, Bi, As, Sb, Al and Ca) were plotted for the average contents of these elements in acidic waters in the oxidation zones of sulfide deposits. The possibility of the formation of Zn, Cd, Ag and Hg selenites under natural oxidation conditions in near surface environments is discussed.

Keywords: selenium minerals; mineral systems; chemical weathering; oxidation zones; physicochemical modeling; Eh–pH diagrams

1. Introduction

Selenium release and pollution is a worldwide phenomenon that results from a wide variety of anthropogenic activities, such as agriculture, mining, and other process industries [1]. Selenium is a potentially toxic element, and mining-related selenium release was a major concern during the last decade as high concentrations were reported at some mine sites [2,3]. Selenium contamination is vast, affecting both aquatic and terrestrial ecosystems, and has therefore attracted the attention of natural resource and water quality regulators around the world [4,5]. Due to the high mobility of selenium in oxidizing geochemical environments, the behavior of selenium is also important in safety analyses of radioactive waste repositories [6,7]. Khamkhash et al. [1] reported a brief introduction to selenium chemistry and toxicity, presented a detailed review of currently available techniques for removing selenium from industrial/mining wastewater, and discussed mining-related selenium contamination from Alaskan mines. Se mobility, bioavailability and toxicity are controlled by the various possible oxidation states (the most common being −2, 0, +4 and +6) that prevail under various conditions. These characteristics of selenium are affected by the redox conditions and the pH, which also plays a crucial role in selenium behavior in near-surface environments.

The oxidation zone of selenide or selenium-bearing sulfide deposits is one of the prime contributors of selenium release into the environment. The mining of coal, precious metals (gold and silver), and metallic sulfides are key contributors of selenium from mining operations [2] exposing selenium-bearing compounds to air and water. This mobilizes selenium into aquatic systems where it bioaccumulates in the food chain, thereby escalating its hazardous effects [1].

Previously, we have characterized the selenium oxysalts (selenites and selenates) and evaluated the accuracy of the thermodynamic constants of the selenites [8]. The objective of this paper is to characterize all selenium minerals as natural mineral systems and to review the thermodynamic constants of the selenium minerals, which are unstable or formed during the oxidation of selenides and selenium-bearing sulfide ores, and to propose data at the standard state (25 °C, 1 bar pressure).

2. Materials and Methods

2.1. Mineral Systems of Selenium Minerals

The selenium minerals are relatively rare in nature; only 118 mineral species are presently known (Supplementary Table S1). As shown [9,10], any mineral can be assigned to a specific system, each component of which is a species-defining chemical element (cf. [11–13]) determined by the rules of the new mineral species definition [14–16]. For mineral coding, we used the sequence of species-defining chemical element symbols according to the so-called "thermochemical" sequence of chemical elements (Figure 1) [9,10]. For example, giraudite, $Cu_6Cu_4Zn_2(AsSe_3)_4S$, responds to the system SSeAsZnCu, while prewittite, $K_2Pb_3Zn_2Cu_{12}(SeO_3)_4O_4Cl_{20}$, responds to the system OClSePbZnCuK.

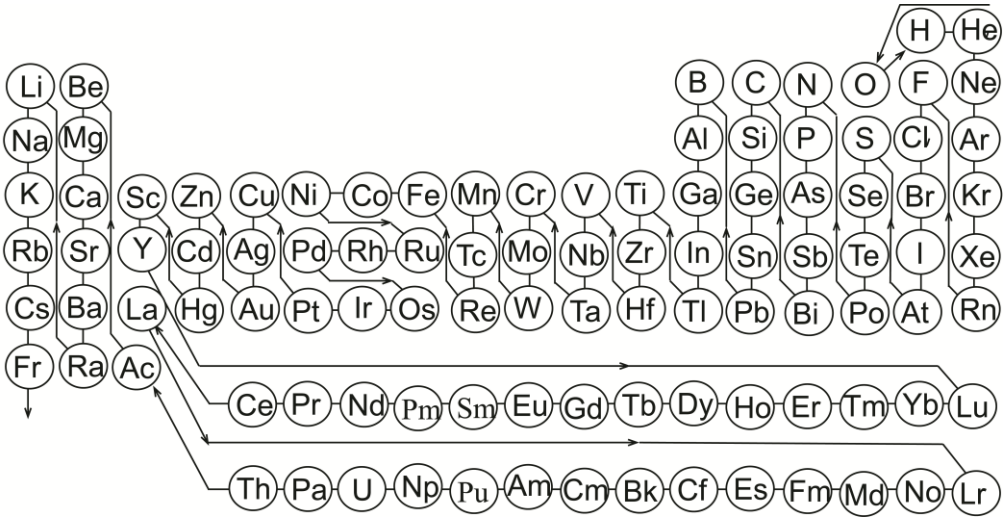

Figure 1. Thermochemical sequence of chemical elements and corresponding single-component systems.

As in all contemporary mineral classifications, selenium minerals is clearly divided into four groups—native selenium, oxide, selenides, and oxysalts—anhydrous selenites (I) and hydrous selenites and selenates (II). Within each of these groups, minerals can be classified according to the minimum number of components required for their formation [9,10]. The proposed classification of selenium mineral systems is given in Table 1. An important advantage of this classification of selenium mineral systems is the ability to use computer technology to organize, store and retrieve thermodynamic data.

Table 1. Mineral systems and $\Delta_f G^0_{298}$ of selenium minerals.

n	System	Mineral	Chemical Formula	$\Delta_f G^0_{298}$, kJ/mol
		Native Elements		
1	Se	Selenium	Se	0
		Oxides		
2	OSe	Downeyite	SeO_2	-171.80 ± 0.62
		Selenides		
2	SeAs	Laphamite	As_2Se_3	-83.9 ± 4.2
	SeSb	Antimonselite	Sb_2Se_3	-127.4 ± 3.7
	SeBi	Nevskite	BiSe	-46.8 ± 5.7
		Guanajuatite	Bi_2Se_3	-146.6 ± 10.1
		Paraguanajuatite	Bi_2Se_3	–
		Laitakarite	Bi_4Se_3	–
	SePb	Clausthalite	PbSe	-97.9 ± 7.7
	SeMo	Drysdallite	$MoSe_2$	–
	SeFe	Achávalite	FeSe	-70.1 ± 4.0
		Dzharkenite (cub)	$FeSe_2$	–
		Ferroselite (orth)	$FeSe_2$	-101.3 ± 15.0
	SeCo	Bornhardtite	$CoCo_2Se_4$	–
		Freboldite	CoSe	-56.3 ± 6.5
		Trogtalite	$CoSe_2$	-100.4 ± 15.0
	SeNi	Sederholmite	NiSe	-69.8 ± 1.6
		Mäkinenite	NiSe	–
		Penroseite	$NiSe_2$	-112.4 ± 7.0
		Kullerudite	$NiSe_2$	–
		Trüstedtite	$NiNi_2Se_4$	–
		Wilkmanite	Ni_3Se_4	–
	SePd	Verbeekite	$PdSe_2$	–
		Oosterboschite	Pd_7Se_5	–
		Palladseite	$Pd_{17}Se_{15}$	–
	SePt	Sudovikovite	$PtSe_2$	–
		Luberoite	Pt_5Se_4	–
	SeCu	Klockmannite	CuSe	-36.8 ± 0.6
		Krut'aite	$CuSe_2$	–
		Petříčekite	$CuSe_2$	–
		Bambollaite	$CuSe_2$	–
		Bellidoite	Cu_2Se	–
		Berzelianite	Cu_2Se	–
		Umangite	Cu_3Se_2	–
		Athabascaite	Cu_5Se_4	
		Geffroyite	Cu_9Se_8	–
	SeAg	Naumannite	Ag_2Se	-46.9 ± 1.3
	SeZn	Stilleite	ZnSe	-172.5 ± 4.0
	SeCd	Cadmoselite	CdSe	-140.9 ± 1.9
	SeHg	Tiemannite	HgSe	-51.2 ± 4.0
3	SSeAg	Aguilarite	Ag_4SeS	–
	SeTeBi	Kawazulite	Bi_2Te_2Se	–
		Skippenite	Bi_2Se_2Te	–
		Telluronevskite	Bi_3TeSe_2	–
		Vihorlatite	$Bi_{24}Se_{17}Te_4$	–
	SeTeNi	Kitkaite	NiTeSe	–
	SeTePd	Miessiite	$Pd_{11}Te_2Se_2$	–
	SeTeAg	Kurilite	Ag_8Te_3Se	–
	SeAsNi	Jolliffeite	NiAsSe	–
	SeAsPd	Kalungaite	PdAsSe	–
	SeAsCu	Mgriite	Cu_3AsSe_3	–
	SeSbPd	Milotaite	PdSbSe	–
	SeSbCu	Bytízite	Cu_3SbSe_3	–
		Permingeatite	Cu_3SbSe_4	–
		Příbramite	$CuSbSe_2$	–

Table 1. *Cont.*

n	System	Mineral	Chemical Formula	$\Delta_f G^0_{298}$, kJ/mol
	SeSbAg	Selenostephanite	$Ag_5(SbSe_3)Se$	–
	SeBiPb	Poubaite	$PbBi_2Se_4$	–
	SeBiPd	Padmaite	$PdBiSe$	–
	SeBiCu	Grundmannite	$CuBiSe_2$	–
		Hansblockite	$CuBiSe_2$	–
		Eldragónite	$Cu_6BiSe_4(Se_2)$	–
	SeBiAg	Bohdanowiczite	$AgBiSe_2$	–
	SePbCu	Schlemaite	Cu_6PbSe_4	–
	SeTlCu	Bukovite	$Cu_4Tl_2Se_4$	–
		Sabatierite	Cu_6TlSe_4	–
		Crookesite	Cu_7TlSe_4	–
	SeFeCu	Eskebornite	$CuFeSe_2$	–
	SeCoCu	Tyrrellite	$CuCo_2Se_4$	–
	SePdCu	Jagüéite	$Cu_2Pd_3Se_4$	–
	SePdAg	Chrisstanleyite	$Ag_2Pd_3Se_4$	–
	SePdHg	Tischendorfite	$Hg_3Pd_8Se_9$	–
	SePtHg	Jacutingaite	Pt_2HgSe_3	–
	SeCuAg	Eucairite	$CuAgSe$	–
		Selenojalpaite	Ag_3CuSe_2	–
	SeCuHg	Brodtkorbite	Cu_2HgSe_2	–
	SeAgAu	Fischesserite	$AgAuSe_2$	–
4	SeAsFeCu	Chaméanite	$(Cu_3Fe)_{\Sigma 4}AsSe_4$	–
	SeSbCuHg	Hakite	$Cu_6Cu_4Hg_2(SbSe_3)_4Se$	–
	SeBiPbCu	Watkinsonite	$Cu_2PbBi_4Se_8$	–
	SeBiPbAg	Litochlebite	$Ag_2PbBi_4Se_8$	–
5	SSeAsZnCu	Giraudite	$Cu_6Cu_4Zn_2(AsSe_3)_4S$	–
	SSeSbCuAg	Selenopolybasite	$CuAg_6Ag_9Sb_2S_9Se_2$	–
	SeBiPbCuHg	Petrovicite	$Cu_3HgPbBiSe_5$	–
		Quijarroite	$Cu_6HgPb_2Bi_4Se_{12}$	–
		I. Selenites without H_2O		
3	OSePb	Molybdomenite	$PbSeO_3$	-458.0 ± 6.0
		Plumboselite	$Pb_3(SeO_3)O_2$	–
4	OSeZn	Zincomenite	$ZnSeO_3$	–
	OSSePb	Olsacherite	$Pb_2(SeO_4)(SO_4)$	–
	OClSeCu	Georgbokiite	$Cu_5(SeO_3)_2O_2Cl_2$	–
		Parageorgbokiite	$Cu_5(SeO_3)_2O_2Cl_2$	–
		Nicksobolevite	$Cu_7(SeO_3)_2O_2Cl_6$	–
		Chloromenite	$Cu_9(SeO_3)_4O_2Cl_6$	–
	OClSeZn	Sofiite	$Zn_2(SeO_3)Cl_2$	–
5	OClSeBiCu	Francisite	$Cu_3Bi(SeO_3)_2O_2Cl$	–
	OClSePbCu	Sarrabusite	$Pb_5Cu(SeO_3)_4Cl_4$	–
		Allochalcoselite	$CuCu_5PbO_2(SeO_3)_2Cl_5$	–
	OClSeCuNa	Ilinskite	$NaCu_5(SeO_3)_2O_2Cl_3$	–
6	OClSeCdCuK	Burnsite	$KCdCu_7(SeO_3)_2O_2Cl_9$	–
7	OClSePbZnCuK	Prewittite	$K_2Pb_3Zn_2Cu_{12}(SeO_3)_4O_4Cl_{20}$	–
		II. Selenites and Selenates Containing H_2O		
4	OHSeAl	Alfredopetrovite	$Al_2(SeO_3)_3{\cdot}6H_2O$	-3657.4
	OHSeCo	Cobaltomenite	$CoSeO_3{\cdot}2H_2O$	-937.4 ± 2.5 [1]
	OHSeFe	Mandarinoite	$Fe_2(SeO_3)_3{\cdot}6H_2O$	-2756.80 ± 7.3
	OHSeNi	Ahlfeldite	$NiSeO_3{\cdot}2H_2O$	-932.4 ± 2.5 [1]
	OHSeCu	Chalcomenite	$CuSeO_3{\cdot}2H_2O$	-835.3 ± 5.3 [2]
	OHSeU	Haynesite	$(UO_2)_3(SeO_3)_2(OH)_2{\cdot}5H_2O$	–
	OHSeCa	Nestolaite	$CaSeO_3{\cdot}H_2O$	-1188.9 ± 2.5

Table 1. *Cont.*

n	System	Mineral	Chemical Formula	$\Delta_f G^0_{298}$, kJ/mol
5	OHClSePb	Orlandiite	$Pb_3(SeO_3)Cl_4 \cdot H_2O$	–
	OHSSeCu	Pauladamsite	$Cu_4(SeO_3)(SO_4)(OH)_4 \cdot 2H_2O$	–
	OHSePbCu	Schmiederite	$Pb_2Cu_2(SeO_3)(SeO_4)(OH)_4$	–
	OHSeCuU	Derriksite	$Cu_4(UO_2)(SeO_3)_2(OH)_6 \cdot H_2O$	–
		Marthozite	$Cu(UO_2)_3(SeO_3)_2O_2 \cdot 8H_2O$	–
	OHSeUCa	Piretite	$Ca(UO_2)_3(SeO_3)_2(OH)_4 \cdot 4H_2O$	–
	OHSeUBa	Guilleminite	$Ba(UO_2)_3(SeO_3)_2(OH)_4 \cdot 3H_2O$	–
	OHSeUNa	Larisaite	$Na(H_3O)(UO_2)_3(SeO_3)_2O_2 \cdot 4H_2O$	–
6	OHSSePbCu	Munakataite	$Pb_2Cu_2(SeO_3)(SO_4)(OH)_4$	–
	OHSeBiPbCu	Favreauite	$PbBiCu_6O_4(SeO_3)_4(OH) \cdot H_2O$	–
	OHSePbCuU	Demesmaekerite	$Pb_2Cu_5(UO_2)_2(SeO_3)_6(OH)_6 \cdot 2H_2O$	–
7	OHISeMgNaK	Carlosruizite	$K_6Na_4Na_6Mg_{10}(SeO_4)_{12}(IO_3)_{12} \cdot 12H_2O$	–

Notes: [1] [17]; [2] [18].

2.2. Thermodynamics

The physico-chemical modeling of mineral equilibria is based on the thermodynamic constants of minerals and aqueous species (values of the Gibbs energy of formation, $\Delta_f G^0_{298}$). These data are mostly calculated from calorimetric measurements (e.g., [19–34]) or experimental determinations of solubility (e.g., [35–44]). Such works are very numerous; their results are not always consistent with each other. A detailed analysis of all thermodynamic data for selenium minerals is beyond the scope of this article; this can be found, for example, in the review [45], and primarily in the reference book [46], which presents a scrupulous critical review of all the published experimental measurements. We used this reference book [46] in the preparation of Table 1, which contains the values of the Gibbs energy of formation ($\Delta_f G^0_{298}$) for selenium minerals and their synthetic analogues. Additional thermodynamic data ($\Delta_f G^0_{298}$ for solid phases not containing selenium and aqueous species) for the calculation of diagrams have been taken from [47]. In addition, some of our recent articles were used as sources of $\Delta_f G^0_{298}$ for certain selenites [17,18,48,49]. It should be emphasized that the values of the Gibbs energy of formation are known only for 25 (Table 1) of the 118 selenium minerals.

3. Results and Discussion

Thermodynamic modeling of the mineral-forming processes in the oxidation zone of ore deposits is based on the analysis of Eh–pH diagrams. In this study, the calculation and construction of Eh–pH diagrams were carried out by means of the Geochemist's Workbench software (GMB 9.0) [50]. The calculation of the diagrams was predated by the introduction of new thermodynamic data and some elements (Cd, Sb, Bi) into the database and the specification of some constants. The activity coefficients were calculated with the Debye–Hückel equation. Eh–pH diagrams of Me–Se–H_2O systems (where Me = Co, Ni, Fe, Cu, Pb, Zn, Cd, Hg, Ag, Bi, As, Sb, Al and Ca) have been constructed for the average contents of these elements in acidic waters of the oxidation zones of sulfide deposits [51]. It should be noted that Eh–pH diagrams of Me–Se–H_2O systems (where Me = Co, Ni, Fe, Cu, Pb, Zn, Al and Ca) have been discussed in detail previously [8] and therefore we present here only their brief description.

3.1. Thermodynamic System Co–Se–H_2O

In this system, three selenides (bornhardtite, $CoCo_2Se_4$; freboldite, CoSe; and trogtalite, $CoSe_2$) and one selenite (cobaltomenite, $CoSeO_3 \cdot 2H_2O$) were reported. For cobalt selenides the thermodynamic data are known only for trogtalite and freboldite (Table 1). These data were used for plotting the Eh–pH diagram of the Co–Se–H_2O system (Figure 2). The thermal stability, solubility and thermochemical calorimetric investigations were carried out on a synthetic analogue of

cobaltomenite [49,52,53]. The Eh–pH diagram of the Co–Se–H_2O system (Figure 2) contains, in addition to the stability field of native selenium, a stability field of Co_3O_4, which is unknown in nature, and the stability field of trogdalite. Cobaltomenite appears in the environment covering the pH range of 4.5 to 7.5, while Eh is not too high.

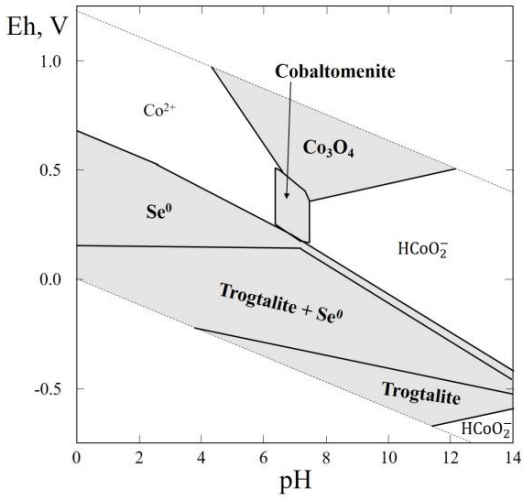

Figure 2. Eh–pH diagram of the system OHSeCo (Co–Se–H_2O) at 25 °C and the activities of the components: $a_{\Sigma Se} = 10^{-4}$, $a_{\Sigma Co} = 10^{-3}$. Here and in Figures 3–15, the solid lines are boundaries of the stability fields of the solid phases.

3.2. Thermodynamic System Ni–Se–H_2O

In this system six selenides (sederholmite, and mäkinenite, NiSe; penroseite, and kullerudite, $NiSe_2$; trüstedtite, and wilkmanite, $NiNi_2Se_4$) were reported, but the thermodynamic data are known only for penroseite and sederholmite (Table 1). These data were used for plotting the Eh–pH diagram of the Ni–Se–H_2O system (Figure 3). The thermal stability, the solubility and the thermochemical calorimetric investigations were carried out on a synthetic analogue of ahlfeldite [49,52,53]. The Eh–pH diagram of the Ni–Se–H_2O system (Figure 3) contains the stability fields of native selenium, penroseite and sederholmite, and a wide field of bunsenite. Ahlfeldite appears in the environment covering the pH range of 4.3 to 8.2, while the Eh is not too high at the temperature fluctuations corresponding to the environmental conditions.

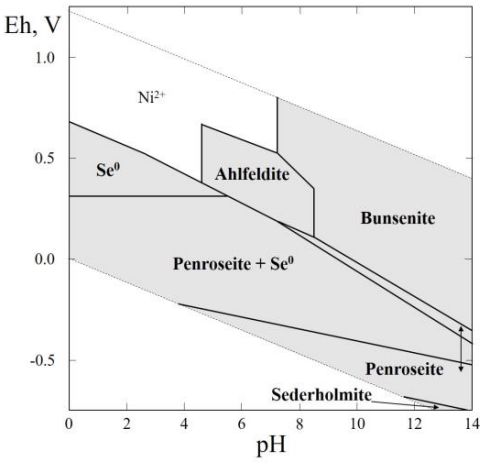

Figure 3. Eh–pH diagram of the system OHSeNi (Ni–Se–H_2O) at 25 °C and the activities of the components: $a_{\Sigma Se} = 10^{-4}$, $a_{\Sigma Ni} = 10^{-2}$.

3.3. Thermodynamic System Fe–Se–H_2O

The Table 1 shows that in this system, three selenides (achávalite, FeSe; dzharkenite, and ferroselite, $FeSe_2$), native selenium, and one selenite, mandarinoite ($Fe_2(SeO_3)_3 \cdot 6H_2O$), were reported. The composition, solubility, and the thermal behavior of iron selenite were discussed earlier [8]. Figure 4 presents Eh–pH diagrams of the Fe–Se–H_2O system, which contains wide stability fields of native selenium, hematite and ferroselite, and small fields corresponding to the crystallization of oxides (magnetite, wüstite). The field of mandarinoite appears in acid areas at a high positive Eh.

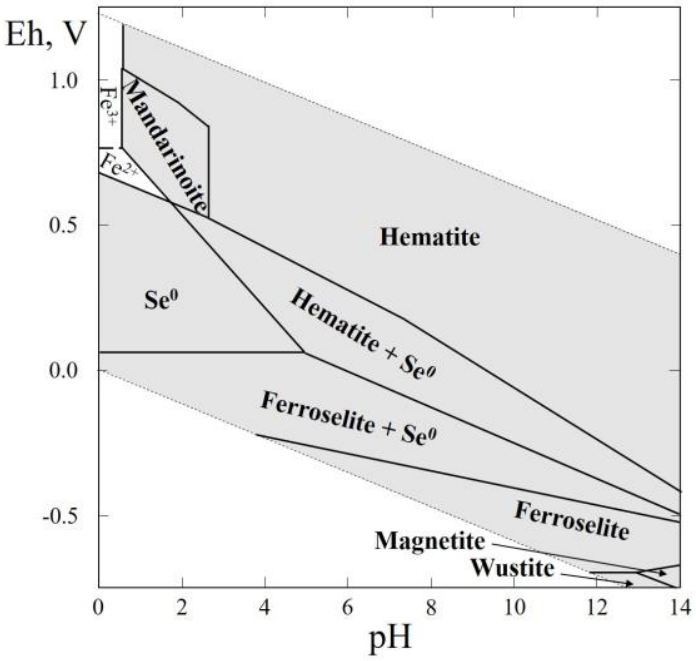

Figure 4. Eh–pH diagram of the OHSeFe (Fe–Se–H_2O) system at 25 °C and the activities of the components: $a_{\Sigma Se} = 10^{-4}$, $a_{\Sigma Fe} = 10^{-2}$. The dotted line is the boundary between fields of Fe^{2+} and Fe^{3+}.

3.4. Thermodynamic System Cu–Se–H_2O

In this thermodynamic system, nine selenides (klockmannite, CuSe; krut'aite, petříčekite, and bambollaite, $CuSe_2$; bellidoite, and berzelianite, Cu_2Se; umangite, Cu_3Se_2; athabascaite, Cu_5Se_4; geffroyite, Cu_9Se_8) were reported, but the thermodynamic data are only available for CuSe (Table 1) and it was used for plotting the Eh–pH diagram of the Cu–Se–H_2O system (Figure 5). Also in this system, two natural polymorphous modifications exist among water-containing selenites without additional anions. They have the $CuSeO_3 \cdot 2H_2O$ formula: chalcomenite (orthorhombic) and clinochalcomenite (monoclinic). Chalcomenite is the more abundant mineral; clinochalcomenite is poorly documented and remains a controversial mineral species. The thermal stability, the solubility and thermochemical calorimetric investigations were carried out on a synthetic analogue of chalcomenite [17,54,55].

The Eh–pH diagram of the Cu–Se–H_2O system is shown in Figure 5. It is seen that klockmannite, copper oxides (cuprite, tenorite), native selenium, and native copper (in the alkaline region of negative Eh) are stable. Chalcomenite ($CuSeO_3 \cdot 2H_2O$) occurs in a slightly acid environment and at a rather high positive Eh.

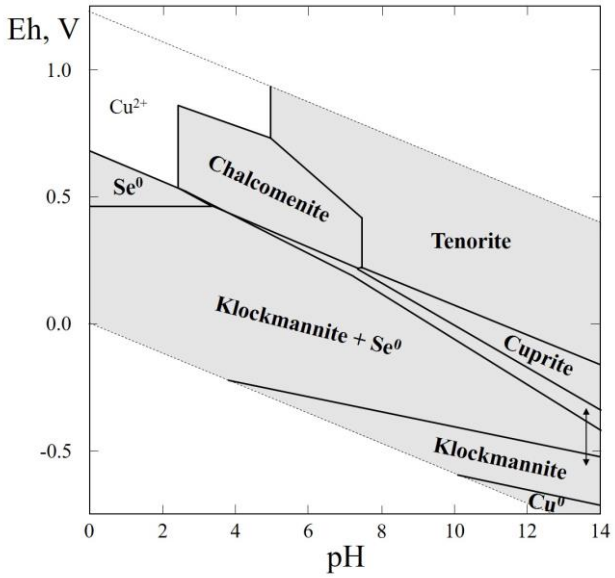

Figure 5. Eh–pH diagram of the OHSeCu (Cu–Se–H_2O) system at 25 °C and the activities of the components: $a_{\Sigma Se} = 10^{-4}$, $a_{\Sigma Cu} = 10^{-2}$.

3.5. Thermodynamic System Pb–Se–H_2O

In this thermodynamic system, one selenide (clausthalite, PbSe), and two anhydrous lead selenites (molybdomenite, $PbSeO_3$, and plumboselite, $Pb_3(SeO_3)O_2$) were reported (Table 1), but the thermodynamic data are only available for PbSe, and $PbSeO_3$ (Table 1). These data were used for plotting the Eh–pH diagram of the Pb–Se–H_2O system (Figure 6). The greatest part of the diagram contains stability fields of solid phases and is characterized by the fields of native selenium, claustalite (PbSe), plattnerite (PbO_2), litharge (Pb_3O_4) and massicot (PbO). It is noteworthy that a wide stability field of molybdomenite ($PbSeO_3$) appears covering the pH range of 4 to 9.5.

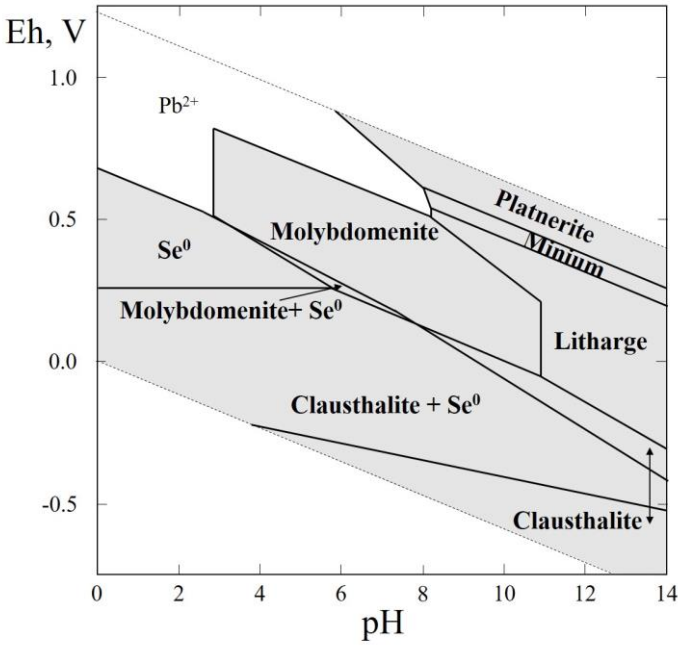

Figure 6. Eh–pH diagram of the OSePb (Pb–Se–H_2O) system at 25 °C and the activities of the components: $a_{\Sigma Se} = 10^{-4}$, $a_{\Sigma Pb} = 10^{-4}$.

3.6. Thermodynamic System Zn–Se–H_2O

In this system only one selenide, stilleite (ZnSe), was reported (Table 1). Natural hydrous Zn selenites have not yet been found, but their formation in nature is quite possible, for example, in the oxidation zones of Se-bearing sulfide ores, in which sphalerite or stilleite (ZnSe) is a source of Zn. The rarity and difficulty of their identification may explain why hydrous zinc selenites have not yet been detected in nature. However, Pekov et al. [56] have recently found a new anhydrous Zn selenite mineral (zincomenite, $ZnSeO_3$) in fumarole products in the Tolbachik volcano.

The solubility and the thermal behavior of synthetic $ZnSeO_3 \cdot 2H_2O$, and $ZnSeO_3 \cdot H_2O$ were discussed in [55,57]. It was shown that $ZnSeO_3 \cdot 2H_2O$ is a more stable phase than $ZnSeO_3 \cdot H_2O$ under environmental conditions. The monohydrate appears to be a metastable phase. The thermochemical calorimetric investigations were carried out on synthetic zinc selenites, $ZnSeO_3 \cdot 2H_2O$ and $ZnSeO_3 \cdot H_2O$ [18].

Finally, the Eh–pH plot of the Zn–Se–H_2O system is shown in Figure 7. This system attracts interest because it allows the estimation of the physico-chemical parameters of the formation of hydrous Zn selenite. As we see in Figure 7, the diagram contains the stability fields of native selenium, stilleite, zincite (ZnO), and zinc selenite ($ZnSeO_3 \cdot 2H_2O$). As follows from this diagram, the physico-chemical parameters of zinc selenite stability—pH, Eh, and the activities of Zn and Se—are close to those of cobalt and nickel selenites (ahlfeldite and cobaltomenite) [49], and $ZnSeO_3 \cdot 2H_2O$ is the stable phase at the temperature fluctuations corresponding to environmental conditions.

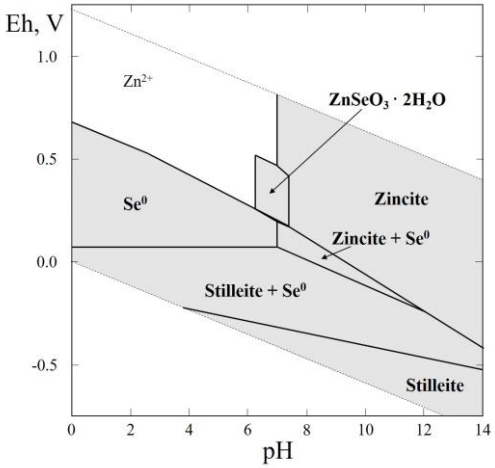

Figure 7. Eh–pH diagram of the OHSeZn (Zn–Se–H_2O) system at 25 °C and the activities of the components: $a_{\Sigma Se} = 10^{-4}$, $a_{\Sigma Zn} = 10^{-2}$.

3.7. Thermodynamic System Cd–Se–H_2O

In this thermodynamic system, only one selenide (cadmoselite, CdSe) was reported (Table 1). Cadmoselite was found in Ust' Uyok deposit (Turan District, Tuva Republic, Eastern-Siberian Region, Russia) as fine xenomorphic disseminations cementing sandstone associated with ferroselite, clausthalite, amorphous selenium, Cd-bearing sphalerite, and pyrite [58]. The thermodynamic constants of synthetic hydrous cadmium selenite were reported [18]. These data were used for plotting the Eh–pH diagram of the Cd–Se–H_2O system (Figure 8). The greatest part of the diagram contains stability fields of solid phases and is characterized by the fields of native selenium, cadmoselite and hydrous Cd selenite. It is noteworthy that a wide stability field of hydrous Cd selenite ($CdSeO_3 \cdot H_2O$) appears covering the pH range of 2 to 12.5. Therefore, in terms of geochemistry, hydrous cadmium selenite is theoretically able to form in the oxidation zones of Se-bearing sulfide ores, in which Cd-bearing sphalerite (Zn, Cd)S or Cd-bearing is a source of Cd. The rarity and difficulty of their identification may explain why hydrous cadmium selenites have not yet been detected in nature.

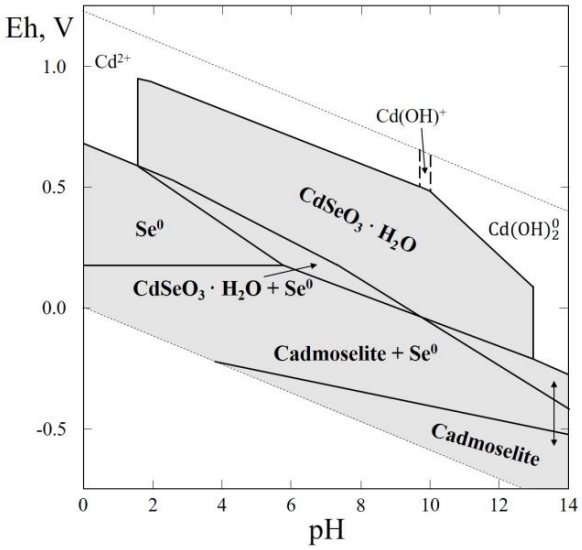

Figure 8. Eh–pH diagram of the OHSeCd (Cd–Se–H_2O) system at 25 °C and the activities of the components: $a_{\Sigma Se} = 10^{-4}$, $a_{\Sigma Cd} = 10^{-2}$. The dotted lines are the boundaries between fields of Cd^{2+}, $Cd(OH)^+$ and $Cd(OH)_2{}^0$.

3.8. Thermodynamic System Hg–Se–H_2O

In this thermodynamic system, one selenide, tiemannite (HgSe) was reported. Natural Hg selenites have not yet been found in nature. Tiemannite was described for the first time at the St Lorenz Mine, Burgstatt veins, Clausthal-Zellerfeld, Harz, Lower Saxony, Germany [59] in association with clausthalite, berzelianite, naumannite, pyrite, sphalerite, galena, quartz, bournonite. Tiemannite is a common mineral, it has been found in 75 localities (according www.mindat.org), associated with low-sulfur hydrothermal deposits with other selenides, and also in mercury deposits. The Eh–pH plots of the Hg–Se–H_2O system are shown in Figure 9. This system is interesting because it allows the estimation of the physico-chemical parameters of the formation of anhydrous Hg selenites. The greatest part of the diagram contains the stability fields of tiemannite, mercury and anhydrous Hg selenites ($HgSeO_3$, Hg_2SeO_3).

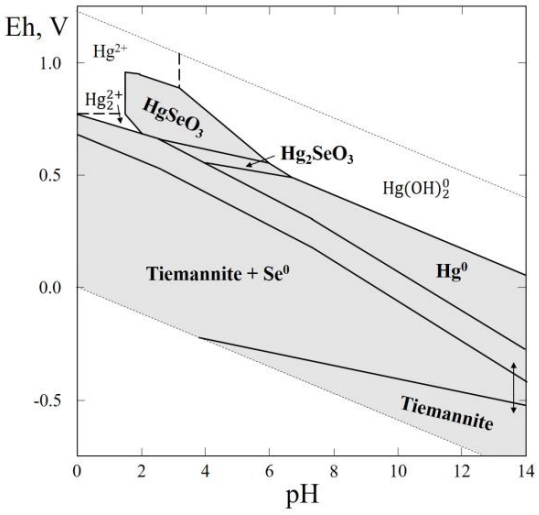

Figure 9. Eh–pH diagram of the OHSeHg (Hg–Se–H_2O) system at 25 °C and the activities of the components: $a_{\Sigma Se} = 10^{-4}$, $a_{\Sigma Hg} = 10^{-5}$. The dotted lines are the boundaries between fields of Hg^{2+}, $Hg_2{}^{2+}$, and $Hg(OH)_2{}^0$.

3.9. Thermodynamic System Ag–Se–H_2O

In this thermodynamic system, only one mineral, naumannite (Ag_2Se) was reported. Naumannite was found in Germany, in the Harz Mountains, at Tilkerode [60], in hydrothermal veins deficient in sulfur, associated with other selenides, quartz, and carbonates. Natural Ag selenites have not yet been found, but their formation in nature is quite possible in the oxidation zones of Se-bearing sulfide ores, because naumannite is a widespread mineral (according to mindat.org it was discovered in 156 localities). The thermodynamic data recommended in the directory [46] was used for plotting the Eh–pH diagram of the Ag–Se–H_2O system (Figure 10). The greatest part of the diagram contains stability fields of naumannite, native selenium and silver, with small field of Ag_2O in extremely alkaline areas at a high positive Eh. It is noteworthy that a small stability field of Ag selenite (Ag_2SeO_3) appears covering the pH range of 6 to 7.5.

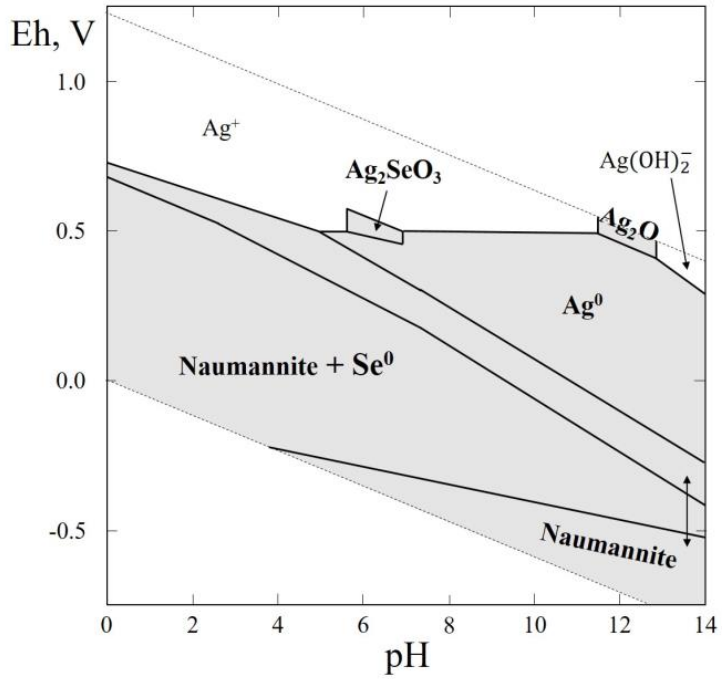

Figure 10. Eh–pH diagram of the OHSeAg (Ag–Se–H_2O) system at 25 °C and the activities of the components: $a_{\Sigma Se} = 10^{-4}$, $a_{\Sigma Ag} = 10^{-5}$.

3.10. Thermodynamic System Bi–Se–H_2O

The Table 1 shows that in this system four mineral species—nevskite (BiSe), guanajuatite (Bi_2Se_3), paraguanajuatite (Bi_2Se_3), and laitakarite (Bi_4Se_3)—were reported, but only for two of them (nevskite and paraguanajuatite) are the thermodynamic data available (Table 1). Both minerals occur in hydrothermal deposits of low to medium temperatures. The greatest part of the Eh–pH diagram of Bi–Se–H_2O system is characterized by the fields of paraguanajuatite, native selenium, and a small bismuth stability field. It is noteworthy that a wide stability field of paraguanajuatite appears covering the wide pH range (Figure 11).

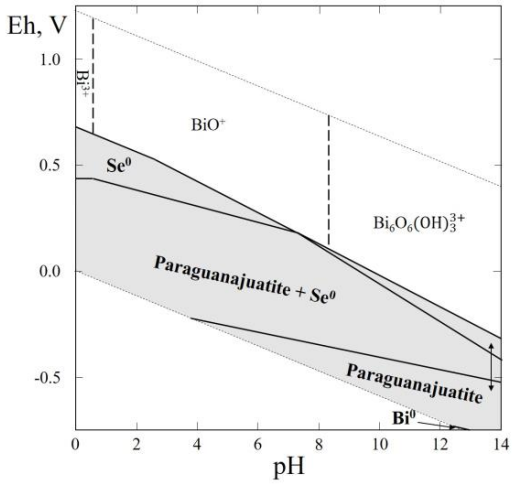

Figure 11. Eh–pH diagram of the OHSeBi (Bi–Se–H_2O) system at 25 °C and the activities of the components: $a_{\Sigma Se} = 10^{-4}$, $a_{\Sigma Bi} = 10^{-5}$. The dotted lines are the boundaries between fields of B^{3+}, BiO^+ and $Bi_6O_6(OH)_3{}^{3+}$.

3.11. Thermodynamic System As–Se–H_2O

In this system only one selenide mineral (laphamite, As_2Se_3) was reported. Laphamite was found in one locality (Burnside, Northumberland County, PA, USA) as a secondary incrustation, probably by sublimation, on a burning pile of waste material from an anthracite coal mine in association with arsenolite, bararite, downeyite, galena, orpiment, selenium, and sulfur [61].

The Eh–pH diagram of the As–Se–H_2O system (Figure 12) shows that the larger part of the diagram contains stability fields of native selenium and laphamite. A small stability field of arsenic corresponds to the alkaline region with a negative Eh.

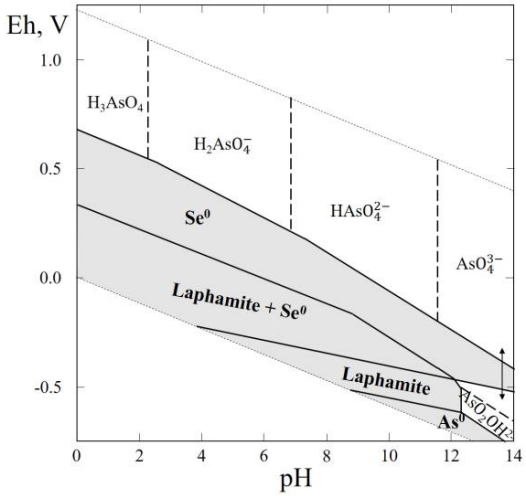

Figure 12. Eh–pH diagram of the OHSeAs (As–Se–H_2O) system at 25 °C and the activities of the components: $a_{\Sigma Se} = 10^{-4}$, $a_{\Sigma As} = 10^{-3}$. The dotted lines are the boundaries between fields of $H_3AsO_4{}^0$, $H_2AsO_4{}^-$, $HAsO_4{}^{2-}$ and $AsO_4{}^{3-}$.

3.12. Thermodynamic System Sb–Se–H_2O

In this system only one selenide, antimonselite (Sb_2Se_3), was reported (Table 1). Antimonselite was found in uraniferous calcite veins in a hydrothermal U–Hg–Mo polymetallic deposit in association

with pyrite, sphalerite, galena, ferroselite, clausthalite, uraninite, cinnabar, hematite, and calcite (near Kaiyan, Guizhou Province, China) [62].

The Eh–pH diagram of the Sb–Se–H_2O system (Figure 13) shows that the larger part of the diagram contains stability fields of antimonselite and native selenium.

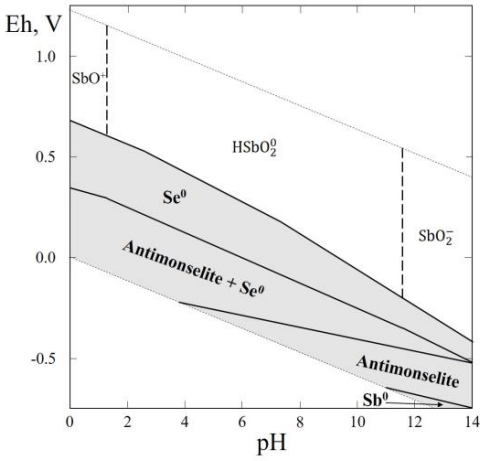

Figure 13. Eh–pH diagram of the OHSeSb (Sb–Se–H_2O) system at 25 °C and the activities of the components: $a_{\Sigma Se} = 10^{-4}$, $a_{\Sigma Sb} = 10^{-5}$. The dotted lines are the boundaries between fields of SbO^+, $HSbO_2{}^0$ and SbO_2.

3.13. Thermodynamic System Al–Se–H_2O

Recently, the compound $Al_2(SeO_3)_3 \cdot 6H_2O$ was found in nature as the mineral alfredopetrovite (Table 1). The mineral occurs in the El Dragón mine, Antonio Quijarro Province, Potosí Department, Bolivia. The El Dragón mine is situated in a telethermal deposit consisting of a single selenide vein hosted by sandstones and shales. Selenide oxidation has produced a wide range of secondary rare selenites (ahlfeldite, chalcomenite, mandarinoite, favreauite, molybdomenite, olsacherite, schmiederite and others), one of which is alfredopetrovite [63].

The Eh–pH diagram of the Al–Se–H_2O system is shown in Figure 14. At the background concentration of Al and Se, the larger section of the diagram contains stability fields of gibbsite ($Al(OH)_3$) and native selenium. A small stability field corresponds to alfredopetrovite in the diagram's acidic section, with a high positive Eh.

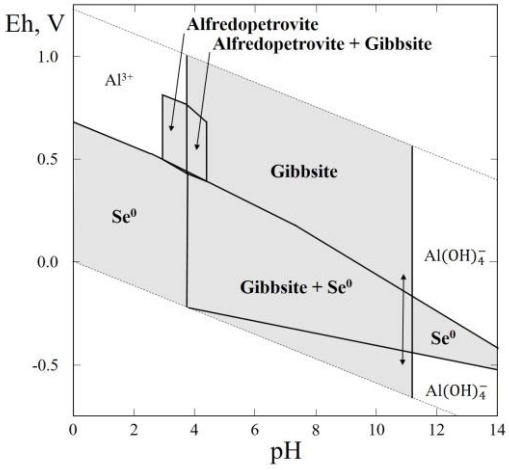

Figure 14. Eh–pH diagram of the OHSeAl (Al–Se–H_2O) system at 25 °C and the activities of the components: $a_{\Sigma Se} = 10^{-4}$, $a_{\Sigma Al} = 10^{-3}$.

3.14. Thermodynamic System Ca–Se–H_2O

In this system, hydrous calcium selenite ($CaSeO_3 \cdot H_2O$) has recently been found in nature as the mineral nestolaite (Table 1). Specimens containing nestolaite were collected in the Little Eva mine, Yellow Cat District, Grand County, UT, USA. The mineral is very rare and occurs as light violet, round aggregations on sandstone associated with cobaltomenite, gypsum, orschallite, ferroselite, native selenium and others. Nestolaite was formed due to the supergene oxidation of primary Se minerals, such as native selenium and ferroselite [64].

The Eh–pH diagram of the Ca–Se–H_2O system is shown in Figure 15. The larger part of the diagram contains stability fields of native selenium and portlandite, $Ca(OH)_2$. A stability field of nestolaite corresponds to the alkaline region with a positive Eh.

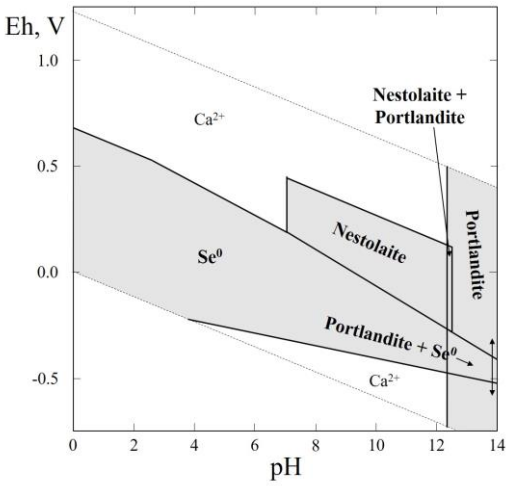

Figure 15. Eh–pH diagram of the OHSeCa (Ca–Se–H_2O) system at 25 °C and the activities of the components: $a_{\Sigma Se} = 10^{-4}$, $a_{\Sigma Ca} = 10^{-2}$.

3.15. Selenates

In conclusion, we dwell on the probable formation of natural Co, Ni, Fe, Cu, Zn and Pb selenates. We calculated the Eh–pH diagrams within a wide range of activities of the components and found values corresponding to the appearance of the stability fields of $CoSeO_4 \cdot 6H_2O$, $CuSeO_4 \cdot 5H_2O$, $NiSeO_4 \cdot 6H_2O$, $PbSeO_4$ and $ZnSeO_4 \cdot 6H_2O$ [65].

The calculations indicate that, among all the discussed systems, selenates are formed only in the Pb–Se–H_2O and Cu–Se–H_2O systems at 25 °C with more or less real (although high) activities of metals and Se in the solution: $a_{\Sigma Se} = 10^{-3}$ and $a_{\Sigma Pb} = 10^{-3}$; $a_{\Sigma Se} = 10^{-1}$ and $a_{\Sigma Cu} = 10^{-1}$.

The activities of Co, Ni and Zn necessary for the formation of their selenate hydrates are extremely high and cannot be encountered in nature. The Eh–pH diagrams of the Cu–Se–H_2O and Pb–Se–H_2O systems show crystallization fields of $CuSeO_4 \cdot 5H_2O$ and $PbSeO_4$ [65]. The results are consistent with the list of the three known mineral species containing selenate ions: schmiederite ($Pb_2Cu_2(SeO_3)(SeO_4)(OH)_4$); olsacherite ($Pb_2(SeO_4)(SO_4)$), which is found at the Dragon and Pacajake deposits in Bolivia and the Baccu Locci deposit in Sardinia, Italy together with selenites; and carlosruizite ($K_6Na_{10}Mg_{10}(IO_3)_{12}(SeO_4)_{12} \cdot 12H_2O$), a very specific mineral differing in its formation conditions, which are found at a niter deposit in association with nitratine, fuenzalidaite, and halite [66]. Kerstenite, $PbSeO_4$ [67], a single simple selenate, has turned out to be a molybdomenite after a detailed study [68].

3.16. Thermodynamic Data

Unfortunately, for most selenium minerals no data on the thermodynamic functions of the formation have been reported. Additional experimental investigations are needed in order to produce reliable and accurate standard thermodynamic data, which will enable researchers to adequately describe Se migration behavior in the oxidation zones of sulfide and selenide ores and contaminated areas. It should be noted that the experimental determination of the thermodynamic data of rare minerals in general, and of the title compounds in particular, on the basis of studying their solubility or by calorimetric measurements, can hardly rely on natural samples, because these usually do not occur in sufficient amounts, forming only tiny crystals which may incorporate inclusions, be covered by weathering crusts, and almost inevitably contain impurities. All these defects influence many properties of the samples studied and certainly their thermodynamic parameters. Therefore, the investigation of the thermodynamic properties of selenium minerals is carried out on their synthetic analogues.

4. Conclusions

The obtained data show that the behavior of selenium, the nearest geochemical counterpart of sulfur, in the surface environment can be quantitatively explained by variations of the redox potential and the acidity–basicity of the mineral-forming medium. Precisely these parameters determine the migration ability of selenium compounds and their precipitation in the form of various solid phases.

Supplementary Materials: The following are available online at www.mdpi.com/2075-163X/7/10/188/s1, Table S1: Selenim minerals: Chemical formula, type locality (TL) and number of localities (NL).

Acknowledgments: The three anonymous reviewers are thanked for their useful comments, which led to many important clarifications. This study was supported by St. Petersburg State University (Grants No. 3.38.286.2015; 3.42.732.2017) and the Russian Foundation for Basic Research (Grant No. 16-05-00293). The St. Petersburg State University Resource Centers "X-Ray Diffraction Methods" and "Geomodel" made their equipment available for this study.

Author Contributions: Vladimir Krivovichev and Marina Charykova wrote the article. Marina Charykova and Andrey Vishnevskiy collected the thermodynamic data and calculated the Eh–pH diagrams.

Conflicts of Interest: The authors declare no conflict of interest.

References

1. Khamkhash, A.; Srivastava, V.; Ghosh, T.; Akdogan, G.; Ganguli, R.; Aggarwal, S. Mining-Related Selenium Contamination in Alaska, and the State of Current Knowledge. *Minerals* **2017**, *7*, 46. [CrossRef]
2. Lemly, A.D. Aquatic selenium pollution is a global environmental safety issue. *Ecotoxicol. Environ. Saf.* **2004**, *59*, 44–56. [CrossRef]
3. Sandy, T.; DiSante, C. *Review of Available Technologies for the Removal of Selenium from Water*; Technical Report; CH2M Hill: Englewood, CO, USA, June 2010; pp. 2–223.
4. Plant, J.A.; Bone, J.; Voulvoulis, N.; Kinniburgh, D.G.; Smedley, P.L.; Fordyce, F.M.; Klinck, B. Arsenic and selenium. In *Environmental Geochemistry*; Treatise on Geochemistry; Holland, H.D., Turekain, K.K., Eds.; Elsevier: Oxford, UK, 2014; Volume 11, pp. 13–57.
5. Sharma, V.K.; McDonald, T.J.; Sohn, M.; Anquandah, G.A.K.; Pettine, M.; Zboril, R. Biogeochemistry of selenium: A review. *Environ. Chem. Lett.* **2014**, *13*, 49–58. [CrossRef]
6. Séby, F.; Potin-Gautier, M.; Giffaut, E.; Donard, O.F.X. Assessing the speciation and the biogeochemical processes affecting the mobility of selenium from a geological repository of radioactive wastes to the biosphere. *Analysis* **1998**, *26*, 193–198. [CrossRef]
7. Chen, F.; Burns, P.C.; Ewing, R.C. ^{79}Se: Geochemical and crystallo-chemical retardation mechanisms. *J. Nucl. Mater.* **1999**, *275*, 81–94. [CrossRef]
8. Charykova, M.V.; Krivovichev, V.G. Mineral systems and the thermodynamics of selenites and selenates in the oxidation zone of sulfide ores—A review. *Mineral. Petrol.* **2017**, *111*, 121–134. [CrossRef]

9. Krivovichev, V.G.; Charykova, M.V. *Classification of Mineral Systems*; St.-Petersburg University Press: Saint-Petersburg, Russia, 2013; 196p. (In Russian)
10. Krivovichev, V.G.; Charykova, M.V. Number of minerals of various chemical elements: Statistics 2012 (a new approach to an old problem). *Geol. Ore Depos.* **2014**, *56*, 553–559. [CrossRef]
11. Hawthorne, F.C. The use of end-member charge-arrangements in defining new mineral species and heterovalent substitutions in complex minerals. *Can. Mineral.* **2002**, *40*, 699–710. [CrossRef]
12. Hatert, F.; Burke, E.A.J. The IMA-CNMNC dominant-constituent rule revised and extended. *Can. Mineral.* **2008**, *46*, 717–728.
13. Christy, A.G. Causes of anomalous mineralogical diversity in the Periodic Table. *Mineral. Mag.* **2015**, *79*, 33–49.
14. Nickel, E.H. The definition of a mineral. *Can. Mineral.* **1995**, *33*, 689–690.
15. Nickel, E.H.; Grice, J.D. The IMA Commission on New Minerals and Mineral Names: Procedures and guidelines on mineral nomenclature. *Can. Mineral.* **1998**, *36*, 913–926.
16. Mills, S.J.; Hatert, F.; Nickel, E.H.; Ferraris, G. The standardisation of mineral group hierarchies: Application to recent nomenclature proposals. *Eur. J. Mineral.* **2009**, *21*, 1073–1080. [CrossRef]
17. Charykova, M.V.; Lelet, M.I.; Krivovichev, V.G.; Ivanova, N.M.; Suleimanov, E.V. A calorimetric and thermodynamic investigation of the synthetic analogue of chalcomenite, $CuSeO_3 \cdot 2H_2O$. *Eur. J. Mineral.* **2017**, *29*, 269–277. [CrossRef]
18. Lelet, M.I.; Charykova, M.V.; Krivovichev, V.G.; Efimenko, N.M.; Platonova, N.V.; Suleimanov, E.V. A Calorimetric and Thermodynamic Investigation of Zinc and Cadmium Hydrous Selenites. *J. Chem. Thermodyn.* **2017**, *115*, 63–73. [CrossRef]
19. Boone, S.; Kleppa, O.J. Enthalpies of formation for group IV selenides ($GeSe_2$, $GeSe_2$(am), SnSe, $SnSe_2$, PbSe) by directcombination drop calorimetry. *Thermochim. Acta* **1992**, *197*, 109–121. [CrossRef]
20. Gattow, G.; Schneider, A. Die Bildungsenthalpien im System Kupfer-Selen. *Z. Anorg. Allg. Chem.* **1956**, *286*, 296–306. (In German) [CrossRef]
21. Grønvold, F. High-temperature reaction calorimeter. Enthalpy of formation of iron selenides and nickel selenides at 1050 K. *Acta Chem. Scand.* **1972**, *26*, 2085–2099. [CrossRef]
22. Grønvold, F.; Westrum, E.F., Jr. Heat capacities and thermodynamic functions of iron disulphide (pyrite), iron diselenide, and nickel diselenide from 5 to 350 K. The estimation of standard entropies of transition metal chalcogenides. *Inorg. Chem.* **1962**, *1*, 36–48. [CrossRef]
23. Leshchinskaya, Z.L.; Selivanova, N.M. Thermodynamic properties of calcium selenite. *Tr. Inst.-Mosk. Khim.-Tekhnol. Inst. Im. D.I. Mendeleeva.* **1963**, *44*, 37–40. (In Russian)
24. Leshchinskaya, Z.L.; Selivanova, N.M. Thermodynamic properties of copper selenites. *Zh. Fiz. Khim.* **1965**, *39*, 2430–2434. (In Russian)
25. Leshchinskaya, Z.L.; Selivanova, N.M.; Maier, A.I.; Strel'tsov, I.S.; Muzalev, E.Y. Heat of formation of nickel and cobalt selenites. *Zh. Vses. Khim. O-va Im. D. I. Mendeleeva.* **1963**, *8*, 577–578. (In Russian)
26. Maekawa, T.; Yokokawa, T.; Niwa, K. Enthalpies of mixing in the liquid state. IV. Bi + Se and Sb + Se. *J. Chem. Thermodyn.* **1972**, *4*, 873–878. [CrossRef]
27. Nasar, A.; Shamsuddin, M. Thermodynamic properties of zinc selenide. *Z. Metallkd* **1990**, *81*, 244–246.
28. O'Hare, P.A.G.; Lewis, B.M.; Susman, S.; Volin, K.J. Standard molar enthalpies of formation and transition at the temperature 298.15 K and other thermodynamic properties of the crystalline and vitreous forms of arsenic sesquiselenide (As_2Se_3). Dissociation enthalpies of As-Se bonds. *J. Chem. Thermodyn.* **1990**, *22*, 1191–1206. [CrossRef]
29. Petrova, Z.K.; Kofman, N.A. Heat capacity and some thermodynamic properties of cadmium selenide. *Dokl. Akad. Nauk BSSR* **1976**, *20*, 688–690. (In Russian)
30. Selivanova, N.M.; Leshchinskaya, Z.L.; Klushina, T.V. Physicochemical properties of selenites. I. Thermodynamic properties of silver selenite. *Zh. Phiz. Khim.* **1962**, *36*, 1349–1352. (In Russian)
31. Selivanova, N.M.; Leshchinskaya, Z.L. Physical-chemical properties of selenites. Thermodynamic properties of lead selenite. *Tr. Inst.-Mosk. Khim.-Tekhnol. Inst. Im. D. I. Mendeleeva.* **1962**, *38*, 37–42. (In Russian)
32. Selivanova, N.M.; Leshchinskaya, Z.L.; Maier, A.I.; Strel'tsov, I.S.; Muzalev, E.Y. Thermodynamic properties of nickel selenite dehydrate. *Zh. Fiz. Khim.* **1963**, *37*, 1563–1567. (In Russian)
33. Sirota, N.N.; Petrova, Z.K.; Solovoskii, T.D. Heat capacity of zinc selenide in the 4,2–300 K region. *Dokl. Akad. Nauk BSSR* **1980**, *24*, 214–217. (In Russian)

34. Stolyarova, T.A.; Gavrilov, N.M.; Nekrasov, I.Y. Thermodynamic properties of bismuth selenides. *Geokhimiya* **1990**, *9*, 1367–1374. (In Russian)
35. Chukhlantsev, V.G.; Tomashevsky, G.P. The solubility of the selenites of certain metals. *Zh. Anal. Khim.* **1957**, *12*, 296–302. (In Russian)
36. Chukhlantsev, V.G. Solubility product of selenite of some metals. *Zh. Neorg. Khim.* **1956**, *1*, 2300–2305. (In Russian)
37. Gospodinov, G.; Barkov, D. Das System HgO-SeO_2-H_2O bei 25 und 100 °C. *Z. Phys. Chem. (Munich)* **1991**, *171*, 241–247. (In German) [CrossRef]
38. Slavtscheva, J.; Popova, E.; Gospodinov, G. Untersuchung von Löslichkeit und Löslichkeitsprodukt bei Seleniten der Elemente der IV. Gruppe des Periodensystems. *Z. Chem.* **1984**, *24*, 105–106. (In German) [CrossRef]
39. Slavtscheva, J.; Popova, E.; Gospodinov, G. Untersuchung der Löslichkeit und Bestimmung des Löslichkeitsproduktes von Kupfer-und Silberselenit. *Monatsh. Chem.* **1993**, *124*, 1115–1118. (In German) [CrossRef]
40. Popova, E.; Slavtscheva, J.; Gospodinov, G. Untersuchung der Löslichkeit einiger Phasen des Systems M_2O_3-SeO_2-H_2O der Elemente der 3. Gruppe des Periodensystems der Elemente. *Z. Chem.* **1986**, *26*, 342–343. (In German) [CrossRef]
41. Rai, D.; Felmy, A.R.; Moore, D.A. The solubility product of crystalline ferric selenite hexahydrate and the complexation constant of $FeSeO_3^+$. *J. Solution Chem.* **1995**, *24*, 735–752. [CrossRef]
42. Ripan, R.; Vericeanu, G. Conductimetric determination of the solubility product of some selenites. *Stud. Univ. Babes-Bolyai Chem.* **1968**, *13*, 31–37. (In Romanian)
43. Mehra, M.C.; Gubeli, A.O. The complexing characteristics of insoluble selenides. 1. Silver selenide. *Can. J. Chem.* **1970**, *48*, 3491–3497. [CrossRef]
44. Savenko, V.S. Solubility product of magnesium and calcium selenites. *Zh. Neorg. Khim.* **1995**, *40*, 1254–1256. (In Russian)
45. Séby, F.; Potin-Cautier, M.; Giffaut, E.; Borge, G.; Donard, O.F.X. A critical review of thermodynamic data for selenium species at 25 °C. *Chem. Geol.* **2001**, *171*, 173–194. [CrossRef]
46. Olin, A.; Nolang, B.; Osadchii, E.G.; Ohman, L.-O.; Rosen, E. *Chemical Thermodynamics of Selenium*; Elsevier: Amsterdam, The Netherlands, 2005; 851p.
47. Wagman, D.D.; Evans, W.H.; Parker, V.B.; Schumm, R.H.; Halow, I.; Bailey, S.M.; Churney, K.L.; Nuttall, R.L. The NBS tables of chemical thermodynamic properties: Selected values for inorganic and C1 and C2 organic substances in (SI) units. *J. Phys. Chem. Ref. Data* **1982**, *11* (Suppl. 2), 1–392.
48. Charykova, M.V.; Krivovichev, V.G.; Depmeier, W. Thermodynamics of arsenates, selenites and sulphates in oxidising zone of sulphides ore deposits. Part I: Thermodynamic properties at standard conditions. *Geol. Ore Depos.* **2010**, *52*, 759–770. [CrossRef]
49. Charykova, M.V.; Krivovichev, V.G.; Lelet, M.I.; Yakovenko, O.S.; Suleimanov, E.V.; Depmeier, W.; Semenova, V.V.; Zorina, M.L. A calorimetric and thermodynamic investigation of the synthetic analogues of cobaltomenite, $CoSeO_3 \cdot 2H_2O$, and ahlfeldite, $NiSeO_3 \cdot 2H_2O$. *Am. Mineral.* **2014**, *99*, 742–748. [CrossRef]
50. Bethke, C.M.; Yeakel, S. *The Geochemist's Workbench (Release 9.0)*; LLC: Champaign, IL, USA, 2011; 130p.
51. Krivovichev, V.G.; Charykova, M.V.; Yakovenko, O.S.; Depmeier, W. Thermodynamics of Arsenates, Selenites, and Sulfates in the Oxidation Zone of Sulfide Ores. IV. Eh–pH Diagrams of the Me–Se–H_2O Systems (Me = Co, Ni, Fe, Cu, Zn, Pb) at 25 °C. *Geol. Ore Depos.* **2011**, *53*, 514–527. [CrossRef]
52. Charykova, M.V.; Krivovichev, V.G.; Yakovenko, O.S.; Semenova, V.V.; Semenov, K.N.; Depmeier, W. Thermodynamics of Arsenates, Selenites, and Sulfates in the Oxidation Zone of Sulfide Ores. VI. Solubility of Synthetic Analogs of Ahlfeldite and Cobaltomenite at 25 °C. *Geol. Ore Depos.* **2012**, *54*, 638–646. [CrossRef]
53. Charykova, M.V.; Fokina, E.L.; Krivovichev, V.G.; Yakovenko, O.S.; Klimova, E.V.; Semenova, V.V. Thermodynamics of Arsenates, Selenites, and Sulfates in the Oxidation Zone of Sulfide Ores. X. Thermal Stability and Dehydration Features of Synthetic Analogs of the Cobaltomenite–Ahlfeldite Solid Solution Series. *Geol. Ore Depos.* **2015**, *57*, 570–578. [CrossRef]
54. Fokina, E.L.; Klimova, E.V.; Charykova, M.V.; Krivovichev, V.G.; Platonova, N.V.; Semenova, V.V.; Depmeier, W. Thermodynamics of Arsenates, Selenites, and Sulfates in the Oxidation Zone of Sulfide Ores. VIII. Field of Thermal Stability of Synthetic Analog of Chalcomenite, its Dehydration and Dissociation. *Geol. Ore Depos.* **2014**, *56*, 538–545. [CrossRef]

55. Charykova, M.V.; Krivovichev, V.G.; Ivanova, N.M.; Semenova, V.V. Thermodynamics of Arsenates, Selenites, and Sulfates in the Oxidation Zone of Sulfide Ores. XI. Solubility of Synthetic Chalcomenite Analog and Zinc Selenite at 25 °C. *Geol. Ore Depos.* **2015**, *57*, 691–698. [CrossRef]
56. Pekov, I.V.; Zubkova, N.V.; Yapaskurt, V.O.; Britvin, S.N.; Chukanov, N.V.; Lykova, I.S.; Sidorov, E.G.; Pushcharovsky, D.Y. Zincomenite, $ZnSeO_3$, a new mineral from the Tolbachik volcano, Kamchatka, Russia. *Eur. J. Mineral.* **2016**, *28*, 997–1004. [CrossRef]
57. Charykova, M.V.; Fokina, E.L.; Klimova, E.V.; Krivovichev, V.G.; Semenova, V.V. Thermodynamics of Arsenates, Selenites, and Sulfates in the Oxidation Zone of Sulfide Ores. IX. Physico-chemical Formation Conditions and Thermal Stability of Zinc Selenites. *Geol. Ore Depos.* **2014**, *56*, 546–552. [CrossRef]
58. Bur'yanova, E.Z.; Kovalev, G.A.; Komkov, A.I. The new mineral cadmoselite. *Zap. Vsesojuz. Miner. Obshch.* **1957**, *86*, 626–628. (In Russian)
59. Naumann, C.F. XI. Classe. Galenoide oder Glanze. B. Selenische Glanze. 531. Selenmercur oder Tiemannit. In *Elemente der Mineralogie*; Wilhelm Engelmann: Leipzig, Germany, 1855; p. 425. (In German)
60. Haidinger, W. Zweite Klasse: Geogenide. XIV. Ordnung. Glanze. III. Silberglanz. Naumannit. In *Handbuch der Bestimmenden Mineralogie*; Braumüller and Seidel: Vienna, Austria, 1845; pp. 563–570. (In German)
61. Dunn, P.J.; Peacor, D.R.; Criddle, A.J.; Finkelman, R.B. Laphamite, an arsenic selenide analogue of 557 orpiment, from burning anthracite deposits in Pennsylvania. *Mineral. Mag.* **1986**, *50*, 279–282. [CrossRef]
62. Chen, L.; Zhang, Q.; Li, D.; Wang, G. Antimonselite, a new mineral. *Acta Mineral. Sin.* **1993**, *13*, 7–11. (In Chinese with English abstract)
63. Kampf, A.R.; Mills, S.J.; Nash, B.P.; Thorne, B.; Favreau, G. Alfredopetrovite: A new selenite mineral from the El Dragón mine. *Eur. J. Mineral.* **2016**, *28*, 479–484. [CrossRef]
64. Kasatkin, A.V.; Plášil, J.; Marty, J.; Agakhanov, A.A.; Belakovskiy, D.I.; Lykova, I.S. Nestolaite, $CaSeO_3 \cdot H_2O$, a new mineral from the Little Eva mine, Grand County, Utah, USA. *Mineral. Mag.* **2014**, *78*, 497–505. [CrossRef]
65. Charykova, M.V.; Krivovichev, V.G. Thermodynamics of environmentally important natural and synthetic phases containing selenium. In *Biogenic-Abiogenic Interactions in Natural and Anthropogenic Systems*; Springer-Verlag: Heidelberg, Germany, 2016; pp. 145–155.
66. Krivovichev, V.G.; Depmeier, W. Selenates and selenites: Systems Se-S-H_2O, Pb-Se-S-H_2O, U-Se-H_2O and U-Se-I-H_2O—Thermodynamical analysis and geological applications. *Zap. Ross. Mineral. Obshch.* **2005**, *134*, 1–14. (In Russian)
67. Mandarino, J.A. Natural and synthetic selenites and selenates and their Gladstone-Dale compatibility. *Eur. J. Mineral.* **1994**, *6*, 337–349. [CrossRef]
68. Burke, E.A.J. A Mass Discreditation of GQN Minerals. *Can Mineral.* **2007**, *44*, 1557–1560. [CrossRef]